Terahertz Time-Domain Spectroscopy as an Electric Propulsion Plasma Diagnostic

IEPC-2019-408

Presented at the 36th International Electric Propulsion Conference
University of Vienna • Vienna, Austria
September 15-20, 2019

Nathan P. Brown[1] and Adam M. Steinberg[2]
Georgia Institute of Technology, Atlanta, GA, 30332, U.S.A.

Jason A. Deibel[3]
Wright State University, Dayton, OH, 45435, U.S.A.

Mitchell L.R. Walker[4]
Georgia Institute of Technology, Atlanta, GA, 30332, U.S.A.

The efficacy of terahertz time-domain spectroscopy (THz-TDS) as a noninvasive electric propulsion plasma diagnostic is evaluated and preliminary electron density measurements with the Georgia Tech THz-TDS system are presented. The THz-TDS system operates in a standard pump-probe configuration in which THz radiation is generated by an ultrashort laser pulse striking a low temperature-grown GaAs photoconductive antenna and detected in the time domain by electro-optic sampling with a ZnTe crystal. The system bandwidth spans 0.2 to 3 THz, thereby enabling line-integrated electron density measurements in electric propulsion plasmas with densities on the order of 10^{17} to 10^{22} m^{-3}. A plasma density of $5 \pm 0.2 \times 10^{18}$ m^{-3} is measured by THz-TDS in an argon 13.58 MHz radio frequency inductively coupled discharge operating at a pressure of 100 mTorr and discharge power of 200 W. Insertion of an obstructing 0.25 in-thick M26 grade boron nitride sample into the THz beam path results in a measured plasma density of $3 \pm 0.2 \times 10^{18}$ m^{-3}. The difference between the two measurements are believed to be caused by day-to-day variations in discharge operation and not by the presence of boron nitride in the THz beam path. This preliminary study finds THz-TDS to be a promising diagnostic for noninvasive internal Hall thruster plasma investigations.

Nomenclature

A	=	magnitude of spectral ratio
c	=	speed of light in vacuum
e	=	elementary charge
E_{gen}	=	generated electric field
E_{sam}	=	sample electric field
E_{ref}	=	reference electric field
exp	=	natural exponential function
G	=	spectrometer frequency response
i	=	square root of negative one
$\check{J}$	=	complex current density

[1] Graduate Research Fellow, School of Aerospace Engineering, nbrown44@gatech.edu
[2] Associate Professor, School of Aerospace Engineering, adam.steinberg@gatech.edu
[3] Associate Professor and Chair, Department of Physics, jason.deibel@wright.edu
[4] Professor and Associate Chair, School of Aerospace Engineering, mitchell.walker@ae.gatech.edu

k = real vacuum k-vector magnitude
$\breve{k}$ = complex k-vector magnitude
L = length of sample or plasma
m_e = electron mass
n = real refractive index
$\breve{n}$ = complex refractive index
n_e = electron number density
n_I = imaginary part of complex refractive index
n_R = real part of complex refractive index
t = time
z = position along radiation propagation
α = absorption coefficient
$\breve{\varepsilon}$ = complex dielectric constant
ϵ_0 = permittivity of free space
ε_I = imaginary part of complex dielectric constant
ε_R = real part of complex dielectric constant
Λ_0 = initial electric field amplitude
λ_0 = initial electric field wavelength
Λ_f = resultant electric field amplitude
λ_f = resultant electric field wavelength
ν = electron collision frequency
ξ = spatial displacement of electron
$\breve{\sigma}$ = complex conductivity
Φ = phase of spectral ratio
ω = radiation frequency
ω_p = plasma frequency
$\hat{}$ = indication of Fourier-transformed variable

I. Introduction

THERE is still much to be learned about the plasma physics governing the interior of Hall thrusters and other electric propulsion (EP) devices. However, nonperturbative optical diagnostics used in the EP field, such as laser-induced florescence (LIF), microwave interferometry, Thomson scattering, and optical emission spectroscopy (OES), are unable to directly measure electron properties in plasmas shielded from optical access by boron nitride. The dearth of reliable experimental work investigating electron dynamics in the thruster interior has inhibited verification of theoretical and computational efforts attempting to explain plasma processes, such as anomalous electron mobility, that have thus far eluded complete characterization.

Terahertz time-domain spectroscopy (THz-TDS) is a novel optical diagnostic with the capability to make these previously infeasible direct electron density measurements in plasmas contained by boron nitride. The technique utilizes broadband pulsed THz radiation that is transmittable through boron nitride to measure electron densities on the order of 10^{17} to 10^{22} m^{-3} in a line-integrated fashion. It is relatively insensitive to mechanical vibrations and applicable in plasmas featuring magnetic fields as high as 10 T and electron temperatures up to 1 keV. Previous work has shown THz-TDS can be used to assist in determination of electron density distribution and, owing to its picosecond-scale pulse durations, enables nanosecond-scale time-resolved plasma evolution measurements.[1-11] This paper reviews the necessary theory, details the THz-TDS system at the Georgia Tech High-Power Electric Propulsion Laboratory (HPEPL), and demonstrates the capability of THz-TDS to make electron density measurements through M26 grade boron nitride.

II. Measurement of Electron Density with THz-TDS

A. Review of Standard THz-TDS Analysis Technique

In the classical description of the interaction of electromagnetic radiation with a medium, the electric field of the incident light wave induces charged particle oscillations in the medium, which, in turn, generate an electric field that interferes with and alters the incident light wave. In the simplified case of monochromatic light, the effect of passage through a medium is to produce a resultant electric field of the same frequency but altered wavelength and amplitude.

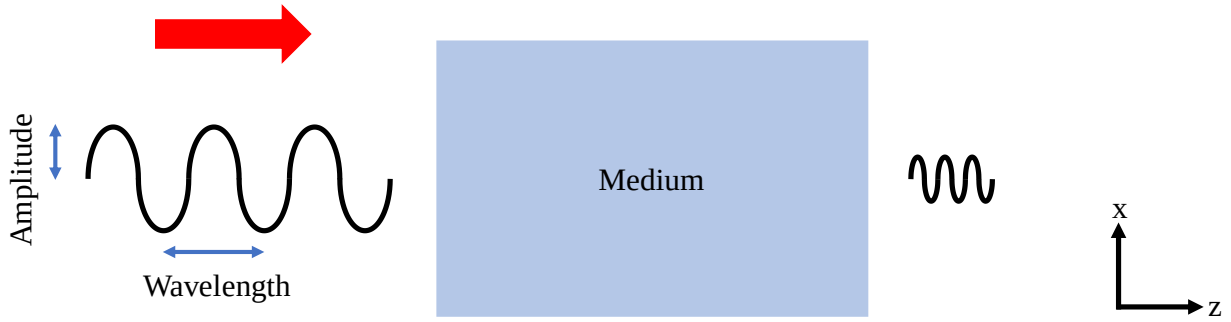

Figure 1. Illustration of interaction between electric field and medium

Changes to the wavelength and amplitude are quantified in terms of the medium refractive index (n) and absorption coefficient (α), respectively, by Eq (1) after propagation through some distance (z) of the medium. The symbols λ_f and Λ_f are the resulting wavelength and amplitude, respectively, and λ_0 and Λ_0 are the incident wavelength and amplitude, respectively.[12]

$$\lambda_f = \frac{\lambda_0}{n}$$
$$\Lambda_f = \Lambda_0 \exp\left(\frac{-\alpha}{2} z\right) \tag{1}$$

THz-TDS measures the frequency-dependent refractive index and absorption coefficient of the sample through which broadband THz radiation is transmitted.[13-16] The electric field of the THz radiation is measured with and without the sample in place to establish sample and reference electric fields, respectively, in the time domain. These fields (E_{sam} and E_{ref}) are converted to the frequency (ω) domain by a Fourier transform (indicated by ˆ) and compared in the form of a transfer function in Eq. (2).

$$\frac{\hat{E}_{sam}(\omega)}{\hat{E}_{ref}(\omega)} = A(\omega) \exp[i\Phi(\omega)] \tag{2}$$

The frequency-dependent magnitude (A) and phase (Φ) of the spectral ratio are related to the sample refractive index and absorption coefficient by Eq. (3), where L is the length of radiation propagation through the sample and c is the speed of light.

$$A(\omega) = \exp\left[-\frac{\alpha(\omega)L}{2}\right]$$
$$\Phi(\omega) = \frac{L\omega}{c}\,[n(\omega) - 1] \tag{3}$$

Derivations of Eqs. (2) and (3) are provided in the Appendix.

B. THz-TDS of Plasma

1. Interaction of THz Radiation with Plasma

In plasmas relevant to EP, the propagation of THz radiation depends exclusively on the number density and collision frequency of plasma electrons. The amplitude and phase of the spectral ratio introduced in Eq. (2) are related to the spatially dependent plasma frequency (ω_p) and collision frequency (ν) of a low temperature plasma by Eq. (4)

if applied magnetic fields are small and if the plasma properties do not vary significantly on the scale of the radiation wavelength. Derivation of Eq. (4) is provided in the Appendix.[17]

$$A(\omega) = \exp\left[-\frac{\omega}{c}\int_0^L \sqrt{-\frac{1}{2}\left(1-\frac{\omega_p^2(z)}{\omega^2+\nu^2(z)}\right)+\frac{1}{2}\sqrt{\left(1-\frac{\omega_p^2(z)}{\omega^2+\nu^2(z)}\right)^2+\left(\frac{\omega_p^2(z)\nu(z)}{\omega[\omega^2+\nu^2(z)]}\right)^2}}\,dz\right]$$

$$\Phi(\omega) = \frac{\omega}{c}\int_0^L \left[\sqrt{\frac{1}{2}\left(1-\frac{\omega_p^2(z)}{\omega^2+\nu^2(z)}\right)+\frac{1}{2}\sqrt{\left(1-\frac{\omega_p^2(z)}{\omega^2+\nu^2(z)}\right)^2+\left(\frac{\omega_p^2(z)\nu(z)}{\omega[\omega^2+\nu^2(z)]}\right)^2}}-1\right]\mathrm{d}z \quad (4)$$

The plasma frequency (in rad/s) is related to the electron number density (n_e), electron charge (e), permittivity of free space (ϵ_0), and electron mass (m_e) by Eq. (5).

$$\omega_p(z) = \sqrt{\frac{n_e(z)e^2}{\epsilon_0 m_e}} \quad (5)$$

The assumptions of low temperature and low applied magnetic field are good in plasmas for which Landau damping is negligible and the electron cyclotron frequency is lower than the radiation frequency. These conditions are strongly satisfied for THz radiation if the plasma electron temperature is less than 1 keV and the applied magnetic field is smaller than 10 T.[17]

2. Determination of Electron Density from Phase Information Alone

Simplifying assumptions are typically made to enable determination of the electron density from phase information alone. Under the assumptions that $\nu \ll \omega_p$ and $\omega_p < \omega$, in which case the plasma acts as a low-loss dielectric with little absorption, the expression inside the first square root in the expression for the phase in Eq. (4) can be expanded to first order with the binomial theorem and assessed in the limit of $\nu^2 \ll \omega^2 - \omega_p^2$ and $\nu^2 \ll \omega^2\left(\omega^2-\omega_p^2\right)^2/\omega_p^4$ to yield Eq. (6).

$$\Phi(\omega) = \frac{\omega}{c}\int_0^L \left[\sqrt{1-\frac{\omega_p^2(z)}{\omega^2}}-1\right]dz \quad (6)$$

The expression inside the square root of Eq. (6) can be further expanded to first order with the binomial theorem in the limit of $\omega_p^2 \ll \omega^2$ to yield Eq. (7).

$$\Phi(\omega) = -\frac{1}{2\omega c}\int_0^L \omega_p^2\,(z)dz \quad (7)$$

Further assumption that the plasma is uniform enables simple computation of the electron density with Eq. (8), the relation used most widely in the microwave interferometry literature.[18] Both the plasma frequency and radiation frequency are in units of rad/s, and the sign preceding Φ depends upon the chosen sign of the exponent in Eq. (2).

$$n_e = -\Phi(\omega)\frac{2\epsilon_0 m_e c\omega}{e^2 L} \tag{8}$$

The assumption of uniform density can be relaxed, as it has been in microwave interferometry work in the EP field, if an appropriate inversion is applied to chordal measurements made in a radially symmetric discharge.[19-23] However, because THz-TDS provides phase information at multiple frequencies, a first-order approximation of electron density profile shape (such as that provided by Langmuir probe data or imaging of plasma fluorescence) can be iteratively optimized by RMS minimization with the measured phases at each THz frequency to determine the electron density profile across the radiation path. In this way, previous work has employed THz-TDS to determine the density profile without need for assumption of symmetry.[2]

III. HPEPL THz-TDS System

THz-TDS can be performed entirely with commercially available equipment. This section reviews the THz-TDS setup at Georgia Tech HPEPL, briefly discusses the physics of operation, and gives system measurement capabilities.

A. System Overview

Diagrammed in Fig. 2, the HPEPL THz-TDS system generates and detects THz radiation in a pump-probe configuration: one beam pumps a photoconductive antenna (PCA) to produce the THz field while the other probes a zinc telluride (ZnTe) crystal to electro-optically detect the THz pulse.

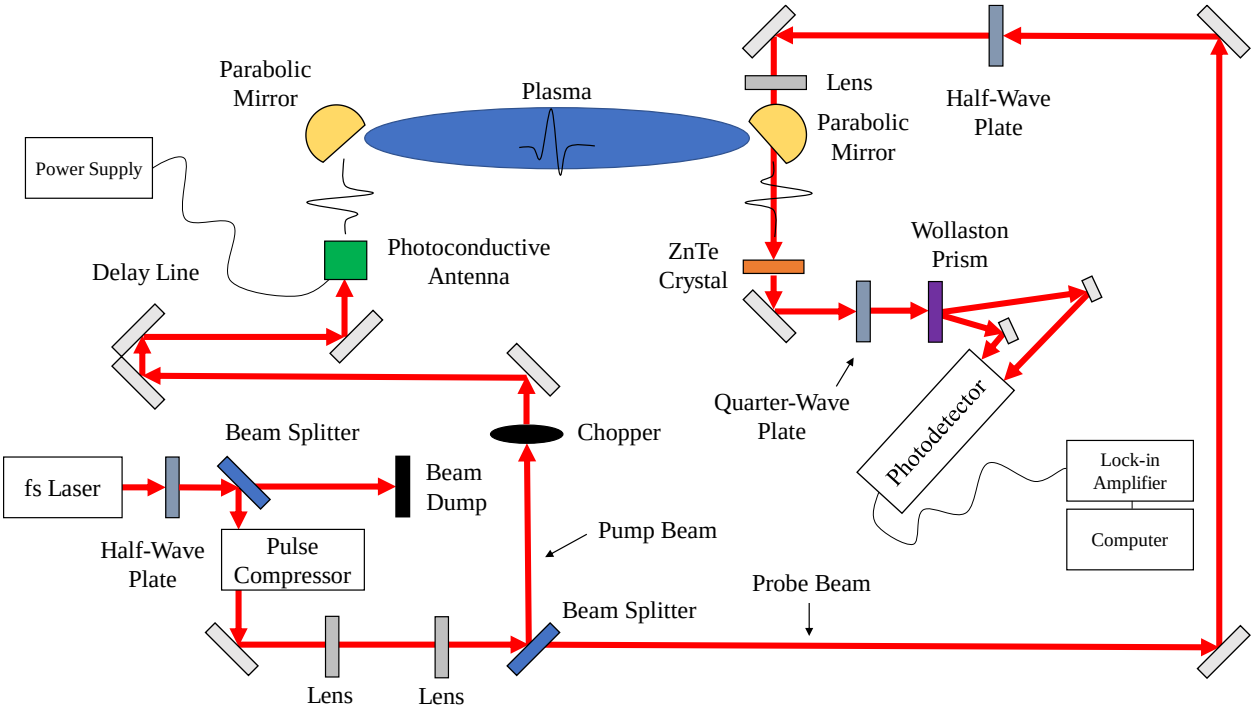

Figure 2. HPEPL THz-TDS system diagram (fs: femtosecond).

The laser beam is provided by a Coherent Vitara-T HP modelocked Ti:Sapphire laser that provides ultrashort pulses with 800 nm center wavelength at a repetition rate of 100 MHz and average power of 1.2 W. The beam then travels through a half-wave plate and polarization-dependent beam splitter to give adjustable control of power inputted into the setup. Next, the beam is guided through a pulse compressor and then recollimated with a pair of lenses before it is split into pump and probe paths by a fixed ratio beam splitter.

The pump beam passes through an optical chopper and then reflects from a hollow corner cube retroreflector mounted on a delay line before reaching the PCA mount. THz radiation emitted from the PCA is collimated to a beam

diameter of approximately 1.4 in and steered into the plasma by a parabolic mirror. After passage through plasma, the THz radiation is focused onto the ZnTe crystal by a second parabolic mirror.

The probe beam is routed through a second half-wave plate to control polarization orientation and then focused through a hole in the second parabolic mirror and onto the ZnTe crystal so that it propagates collinearly with the THz radiation at identical polarization. After passage through the crystal, the probe beam is recollimated and guided through a neutral density filter, quarter-wave plate, and Wollaston prism. The two beams exiting the Wollaston prism are focused onto the two photodiodes of a balanced photodetector. The output of the photodetector is read by a lock-in amplifier connected to a desktop computer running custom LabVIEW software. The optical table is electrically grounded and all instruments are housed in an environmentally controlled enclosure.

B. Physics of Operation

1. Ultrashort Pulse Considerations

The Vitara-T HP provides ultrashort laser pulses with measured temporal full width at half maximum (FWHM) of approximately 30 femtoseconds (fs) at the laser output. The uncertainty principle dictates that such pulses are necessarily spectrally broad and not monochromatic. In this setup, for instance, the measured spectral FHWM is 60 nm. For such pulses, group velocity dispersion (GVD) can have a major impact on temporal pulse width and must be accounted for in the optics setup. GVD occurs because the refractive index of each optical component (and even air) varies as a function of frequency. As a laser pulse travels through a setup, each of its spectral components experiences a different refractive index and therefore travels at a different speed. GVD therefore spectrally separates the pulse in time and thus increases the overall temporal pulse width.[24] Failure to account for GVD in a standard THz-TDS setup can result in pulse lengthening of more than three orders of magnitude.

GVD is mitigated in this setup by use of specially coated low GVD ultrafast mirrors, lenses, beam splitters, and wave plates designed for ultrashort pulses centered at 800 nm. GVD pre-compensation is provided by a Coherent CPC II pulse compressor. Before the beam is split into pump and probe paths, it undergoes multiple reflections from negative GVD-coated mirrors and makes four passes through prism elements in the CPC II. These events serve to lengthen each laser pulse in the opposite manner as the rest of the optical setup: the pulse compressor accelerates the shorter wavelength components ahead of the longer wavelength components to compensate for the tendency of other optics to accelerate longer wavelength components ahead of shorter wavelength components. As illustrated in Fig. 3, the pulse compressor therefore serves to lengthen the pulse duration so that the other optical components provide recompression. Though the pulse width lengthens somewhat through the setup, the aforementioned GVD compensation schemes ensure the measured FHWM temporal pulse width remains less than 50 fs at both the PCA and nonlinear crystal.

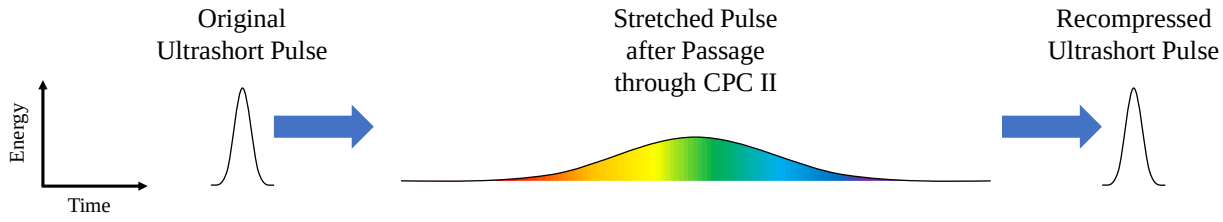

Figure 3. Illustrated ultrashort pulse broadening and recompression.

2. THz Radiation Generation

The PCA used for THz emission is a Menlo Systems TERA8-1 low temperature-grown gallium arsenide (LT-GaAs) wrapped dipole antenna adhered to a printed circuit board. The photoconductive substrate consists of a thin (~ 1 micron) LT-GaAs buffer layer grown atop a much thicker (~380 micron) semi-insulating gallium arsenide (SI-GaAs) region. Gold electrodes patterned onto the LT-GaAs form a 5 micron dipole gap, across which a DC bias of 30 V is applied. The pump beam is limited to an average power of 7 mW to avoid damaging the PCA and is focused onto the gap with an aspheric lens positioned with sub-micron precision by a custom mount assembled with commercially available optomechanical components. Figure 4 features a magnified image of the PCA taken with an Olympus LEXT OLS4100 microscope.

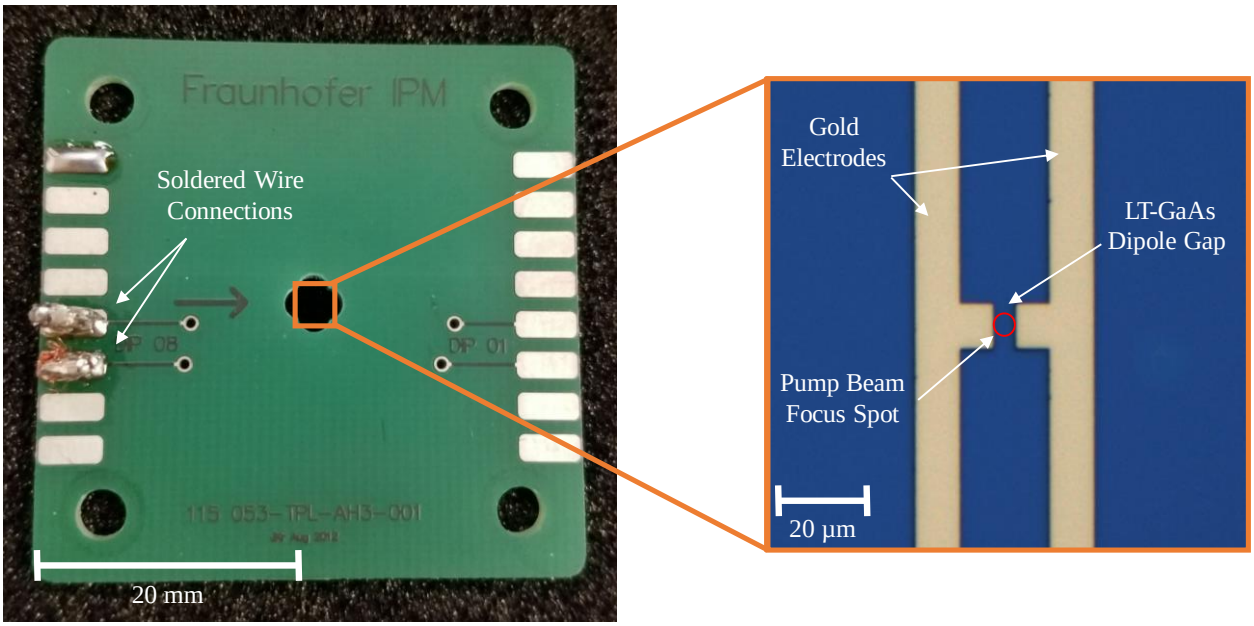

Figure 4. Magnified image of PCA (LT-GaAs: low temperature-grown gallium arsenide).

The ultrashort laser pulses in the pump beam act as a fast switch for the PCA's electrical circuit. Photons impinging on the surface of the antenna are absorbed by the LT-GaAs substrate and excite electrons from the semiconductor's valence band into its conduction band. These newly freed photoelectrons accelerate across the dipole gap in response to the applied voltage bias and thereby produce a transient current that, in turn, alters the local electric field and generates pulsed THz radiation. The process is dependent upon the temporally short nature of both the 50 fs incident laser pulses and 0.2 – 0.3 picosecond (ps) average photoelectron lifetime.[14, 15, 25, 26] Because the dipole gap is much smaller than the THz wavelength, the radiation is highly divergent and therefore coupled to air with a precisely positioned hyper-hemispherical high-resistivity float-zone silicon lens pressed against the SI-GaAs.[27] Figure 5 illustrates the THz generation process from a side view of the PCA.

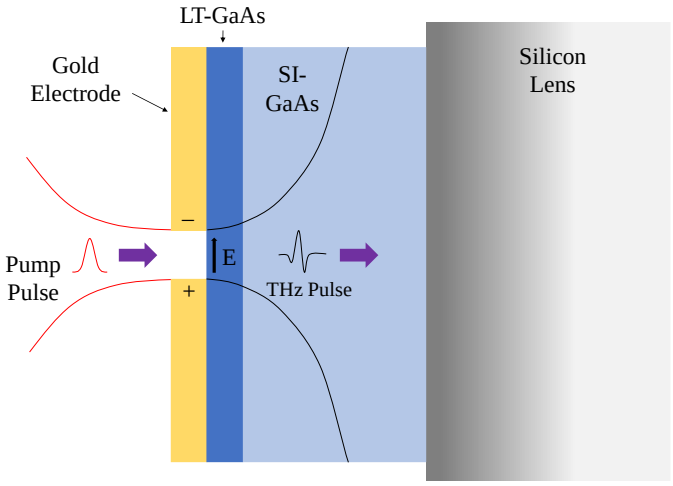

Figure 5. Illustrated THz generation process (not to scale; LT-GaAs: low temperature-grown gallium arsenide, SI-GaAs: semi-insulating gallium arsenide).

3. THz Radiation Detection

After passage through the plasma, the THz radiation is focused onto a 1 mm-thick <110> ZnTe crystal oriented such that propagation is along the [110] axis and polarization is in the direction of the [1 $\bar{1}$ 0] axis. The probe beam

has the same polarization as the THz radiation and is focused onto the ZnTe so that it propagates collinearly through the crystal with the THz beam.[28]

Because ZnTe possesses non-zero electro-optic coefficients, the electric field of the THz radiation induces birefringence in the crystal. This induced birefringence causes the originally linearly polarized copropagating probe pulse to become slightly elliptically polarized to a degree that is linearly proportional to the strength of the THz field. The modified pulse is guided through a quarter-wave plate so that its polarization is shifted from nearly linear to nearly circular and then through a Wollaston prism so that it is split into its two orthogonal polarization components. The intensities of the two components are differenced by a Thorlabs PDB415A-AC balanced photodetector to determine the ellipticity of the probe pulse, and, thus, the relative THz field strength.[14, 15, 29-31] The evolution of probe pulse polarization is illustrated in Fig. 6.

The pump beam is chopped at a typical rate of 1 kHz with a Scitec Instruments 300 CD optical chopper so that the photodetector signal can be extracted from background noise by a Zurich Instruments MFLI lock-in amplifier operating with a typical filter order of 3 and time constant of 61 ms. The high lock-in detection rate (which can be extended up to the 100 MHz output of the laser with appropriate equipment) makes the system relatively insensitive to mechanical noise.

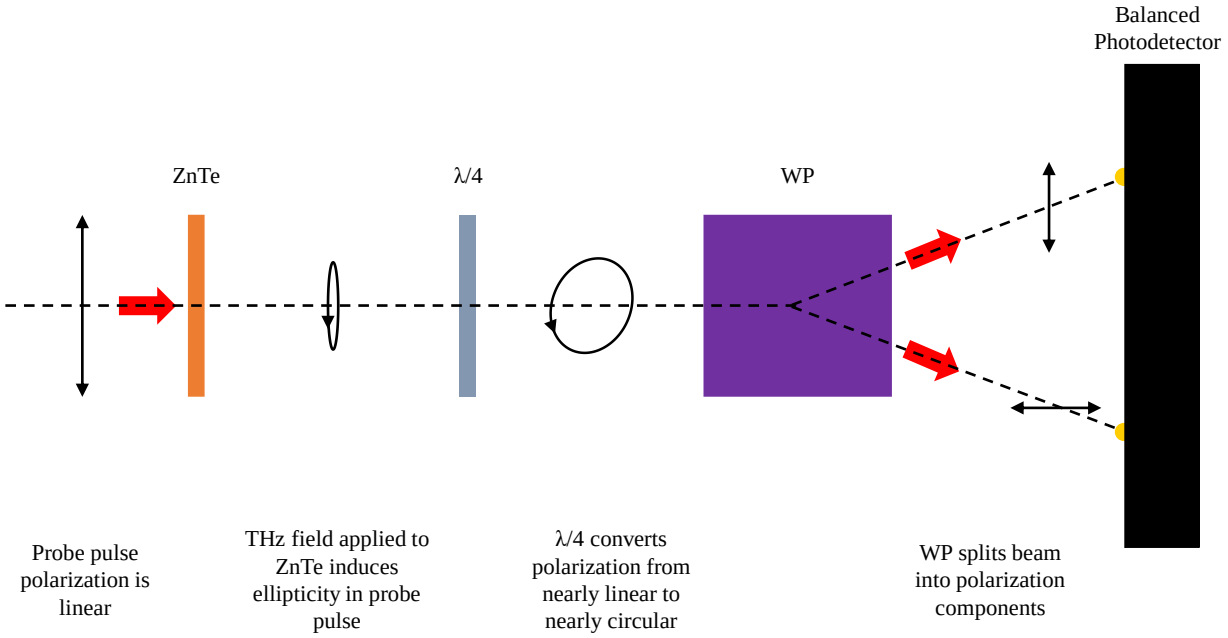

Figure 6. Evolution of probe pulse polarization in THz detection process (ZnTe: zinc telluride crystal, λ/4: quarter-wave plate, WP: Wollaston prism).

Depending on the application, relevant information in the THz field is contained in a duration of 5 to 300 ps. The ultrashort probe beam must therefore be scanned across the duration of the THz pulse for acquisition of the entire field. Scanning is achieved with a Newport DL325 delay line that delays arrival of the pump beam to the PCA, thereby delaying the arrival of each THz pulse to the ZnTe relative to each pulse in the probe beam. The guaranteed position accuracy of the delay line translates to THz field resolution of better than 20 fs, but resolution is ultimately limited in this setup to 50 fs by the temporal FWHM of the ultrashort pulse. Scanning proceeds as follows: the delay line is moved to the desired position; software waits for the lock-in amplifier output to reach its 99% settling time; the signal is acquired as the average of a selectable number of samples over a selectable sampling time; the delay line moves to its next position. Depending on necessary noise suppression and desired scan resolution and length, measurements of the ps-scale THz field require between 10 seconds and 30 minutes of real time. All measurements taken in this paper averaged 1000 samples at each delay line position and required a total time of 5 minutes to resolve the entire THz field. Further work will seek to determine lower limits on required measurement time. Real-time measurement constraints notwithstanding, the short nature of the THz pulse enables extremely high temporal resolution

measurements in repeatable or oscillating plasmas. In these cases, temporal resolution is limited by gating electronics and can be achieved at a nanosecond scale.[1, 2]

C. Measurement Capabilities

A sample pulse generated and detected by the system at HPEPL is shown in Fig. 7. It consists of resolvable frequencies ranging from 0.2 to 3 THz and features a peak signal-to-noise ratio of approximately 170 to 1. Deviations from an ideal THz pulse are caused by electron screening in the PCA, reflections in the ZnTe, and the presence of water vapor in the pulse path, but these do not greatly impact THz-TDS measurement capability and are common in THz-TDS systems.[14, 15, 32]

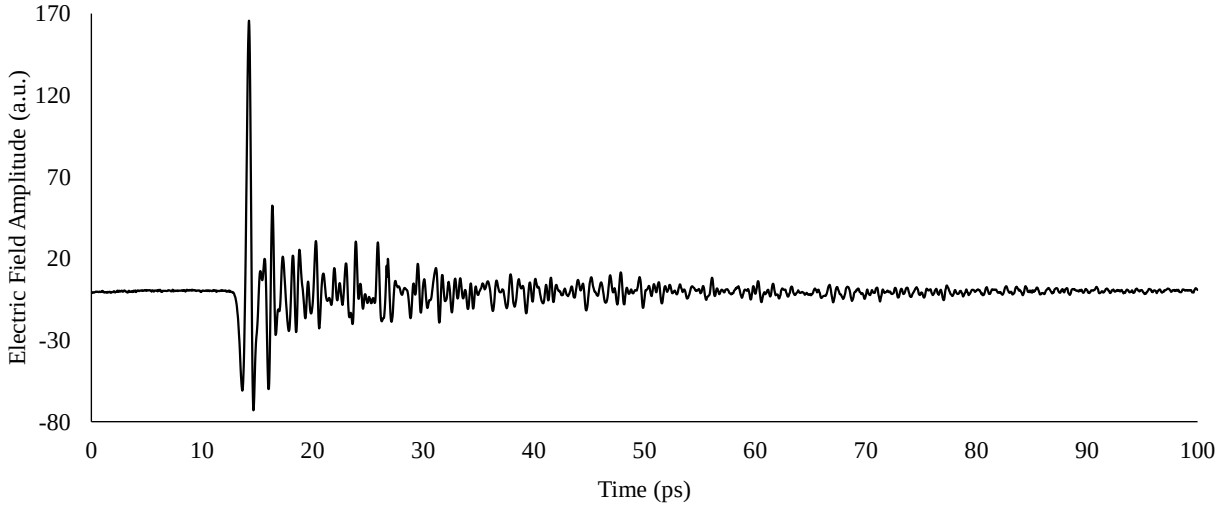

Figure 7. THz pulse generated and measured by HPEPL THz-TDS system.

The maximum electron temperature and applied magnetic field limits required for application of Eq. (4) are much higher than those typically found in Hall thrusters and other EP plasmas.[33] Further assumptions that the plasma frequency is much larger than the electron collision frequency and that the THz radiation frequency is larger than the plasma frequency are also generally satisfied. In fact, only at plasma densities as large as 10^{22} m^{-3} does THz radiation experience plasma cut-off effects.[17] Eq. (7) and, if the plasma can be considered reasonably uniform along the THz path, Eq. (8) are therefore applicable.

Though the theory does not preclude THz-TDS measurements in most EP plasmas, practical considerations place a limit on the lower electron density at which a measurement can be resolved. The smallest resolvable phase (in rad) at each THz frequency is equal to the temporal resolution of the THz field multiplied by the THz radiation frequency (in rad/s). Under the assumption of a uniform plasma, Eq. (8) can be combined with the relation for smallest resolvable phase to determine the lowest resolvable electron number density at each frequency. Figure 8 provides the result of this calculation for the HPEPL system for a plasma length of 10 cm. At the minimum resolvable frequency of 0.2 THz, the lowest resolvable electron density is 1.5×10^{17} m^{-3} across a length of 10 cm. It should be noted that, for shorter plasma lengths, lowest resolvable electron density increases; reducing the plasma length to 1 cm, for instance, increases the lowest resolvable electron density to 1.5×10^{18} m^{-3}. These minima are similar to those of other plasma THz-TDS systems.[8]

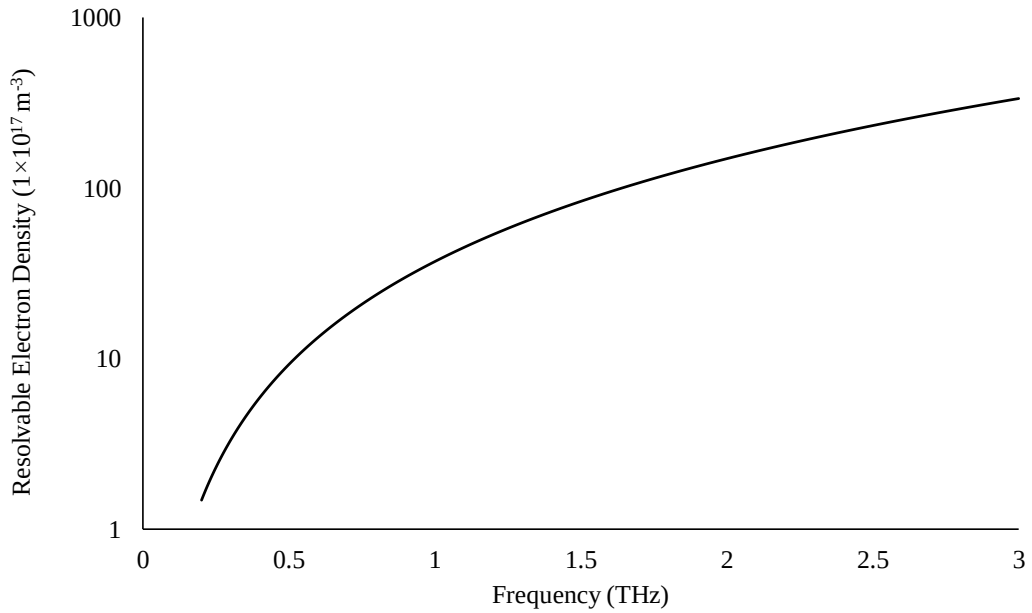

Figure 8. Minimum detectable electron density for a plasma length of 10 cm

D. Estimation of Measurement Uncertainty

Though no published efforts to-date have performed a comprehensive study of uncertainties associated with THz-TDS electron density measurements, a first-order effort to quantify measurement uncertainty is made here. Major expected sources of uncertainty include theoretical resolvable electron density limits, inaccuracies in plasma length measurement, and shot-to-shot variations of the THz pulses caused by changes in lab environment or delay line jitter. Assessment of the uncertainties related to the assumption of uniform plasma required for use of Eq. (8) are not considered here.

Theoretical electron density limits are quantified above and are a function of THz frequency. Because all resolvable frequencies in this work with small enough minimum detectable electron density for use in the RF ICP measurements discussed in Section V measured the same electron density, within their respective resolution limits, the lowest resolvable electron density uncertainty is chosen to be that associated with the lowest resolvable frequency of 0.2 THz. Across the plasma length discussed in Section IV, this uncertainty is approximately 1.1×10^{17} m^{-3}.

Uncertainty of the plasma length measurement is conservatively set to 10% of the total measured length. Previous work by the authors investigating shot-to-shot variation of THz pulses transmitting though the experimental setup without the presence of plasma found differences between various data sets to produce negligibly small measurement uncertainties (on the order of 10^{12} m^{-3}). Therefore, only the impact of lowest resolvable electron density and errors in plasma length measurement are expected to significantly impact measurement uncertainty. The combination of these uncertainties produces a total uncertainty of approximately 2×10^{17} m^{-3}.

IV. Radio Frequency Inductively Coupled Plasma Discharge

A RF ICP discharge provides the plasma testbed for THz-TDS electron density measurements. The discharge, pictured in Figure 9 without its Faraday cage, consists of a quartz tube cross (2 in outer diameter, 16 in length, 5 in width) connected to steel KF vacuum flanges by quick-connect couplings. A rotary vane mechanical pump evacuates the discharge chamber to a base pressure of 1.4 mTorr. RF power is coupled to the plasma via a three-turn hollow copper antenna wrapped around the glass tube. The unbalanced RF signal is generated by a YAESU FT-840 transceiver, amplified by an ACOM 2000A linear amplifier, fed through a Palstar HF-AUTO antenna tuner, and converted to a balanced signal by a DX Engineering BAL450-H10-A current balun connected to the antenna. The discharge is operated at a discharge power of 200 W at 13.58 MHz and pressure of 100 mTorr (corrected for argon). At these conditions, the generated plasma is approximately 14 cm in length. An electrically grounded Faraday cage surrounding the antenna prevents stray electromagnetic radiation or electrical arcs from interfering with THz-TDS measurement equipment. The discharge viewports, manufactured by Torr Scientific, feature Z-cut crystalline quartz

windows that, compared to standard amorphous quartz windows, exhibit relatively low absorption in the THz regime. THz radiation is sent through the longer dimension of the quartz tube.

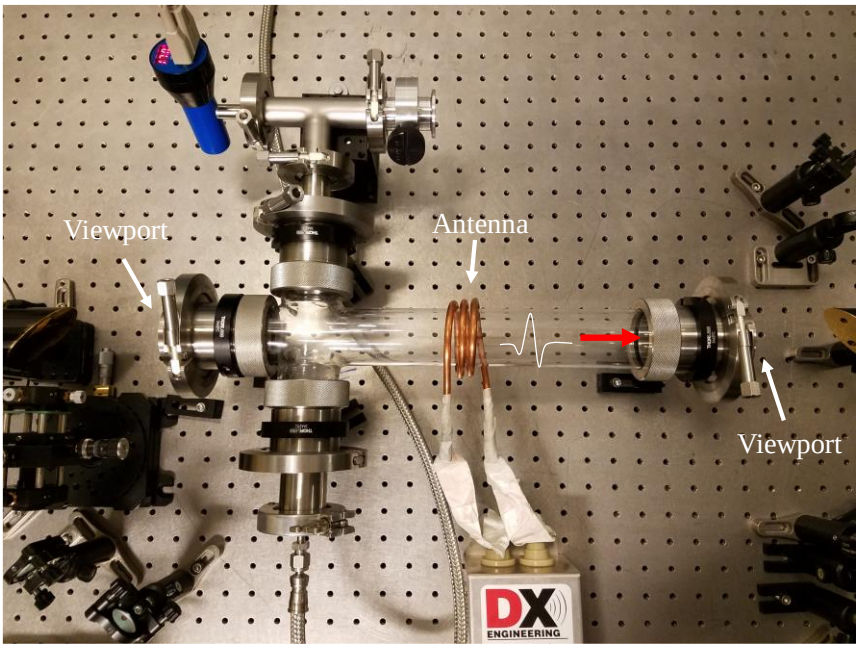

Figure 9. RF ICP discharge

V. Results and Discussion

Demonstration of the HPEPL THz-TDS system as a plasma diagnostic is provided by measurement of electron density in the RF ICP discharge. Because a unique advantage to THz-TDS is the transmissibility of THz radiation through boron nitride, measurements are made both with and without M26 grade boron nitride in the THz beam path.

A. Unobstructed Electron Density Measurement of RF ICP Discharge

THz radiation is first transmitted through the evacuated discharge chamber to establish the reference signal and then through the operating discharge to generate the sample signal. These two signals are shown in Figure 10 and an image of the discharge in operation is shown in Figure 11. Applying Eq. (8) under the simplified assumption of a uniform plasma yields a measured electron density of $5 \pm 0.2 \times 10^{18}$ m^{-3} across all resolvable frequencies from 0.2 to 0.5 THz. Minimum resolvable density limits associated with larger frequencies precludes their use in the density calculation. The measured value is consistent with trends established in published THz-TDS measurements of other ICP discharges operating at higher pressure and power.

It is also interesting to note that, as clearly demonstrated by Figure 10, transmission through plasma accelerates the THz pulse ahead of the vacuum THz pulse. This effect occurs because the plasma refractive index is less than unity. Though this result does imply a THz phase velocity greater than the vacuum speed of light, special relativity is not violated because no photons or information travel faster than this universal speed limit through the plasma.

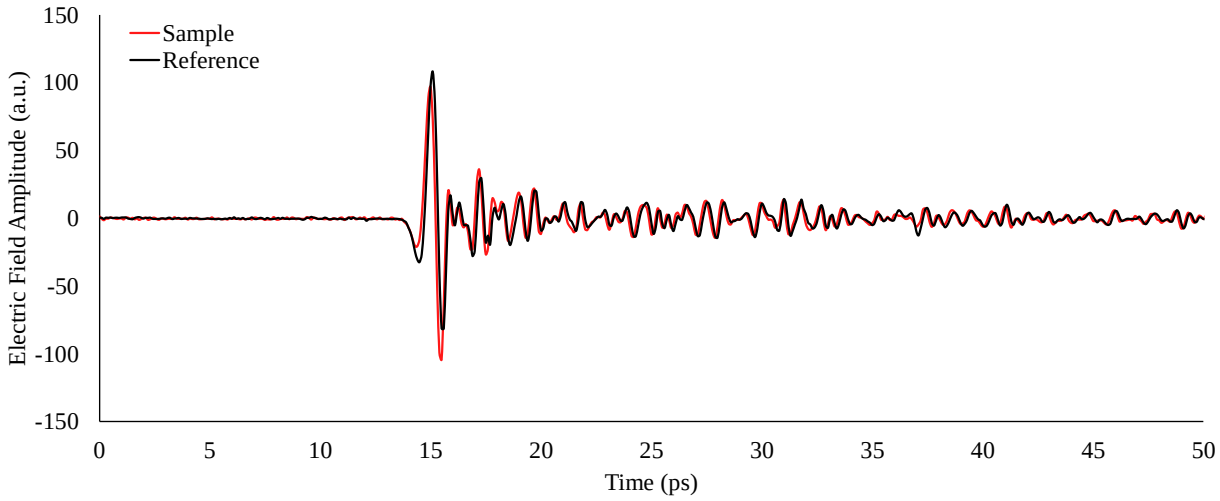

Figure 10. Reference and sample THz signals for unobstructed electron density measurement

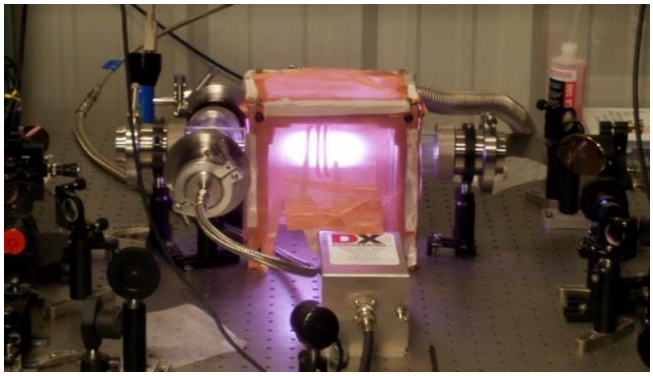

Figure 11. Argon RF ICP discharge operating at 100 mTorr and 200 W.

B. Obstructed Electron Density Measurement of RF ICP Discharge

The THz path to the RF ICP discharge is impeded by a 3 × 2 × 0.25 in sample of M26 boron nitride obtained from Saint-Gobain Ceramics so that, as shown in Figure 12, the THz path is completely obstructed. M26 grade boron nitride is 60% hexagonal close-packed boron nitride and 40% amorphous silica by weight and is used as wall material in Hall thrusters. The sample is oriented such that the THz radiation is transmitted through the 0.25 in dimension and the polarization of the THz radiation is parallel to one of the ordinary axes of the orthotropic boron nitride.

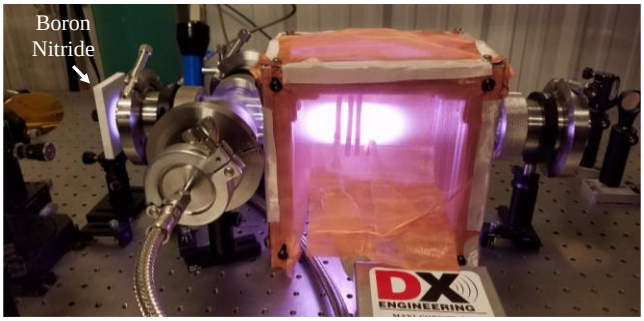

Figure 12. Argon RF ICP discharge operating at 100 mTorr and 200 W with M26 boron nitride impeding THz radiation path.

As in the unobstructed measurement, sample and reference signals are recorded with and without the presence of plasma, respectively, to determine the electron density with Eq. (8). The sample and reference signals are shown in Figure 13 and the measured electron density is $3 \pm 0.2 \times 10^{18}$ m^{-3} across all resolvable frequencies from 0.2 to 0.5 THz. Signal-to-noise ratio is noticeably reduced by the presence of boron nitride in the THz beam path because of absorption, etalon losses, and refraction of beam components away from the original THz path. However, the measured electron density is still of the same order of magnitude as that measured without the impediment of boron nitride. As the two measurements were taken on different days, differences between them are more likely caused by lack of repeatability of the RF ICP discharge than the impediment of boron nitride.

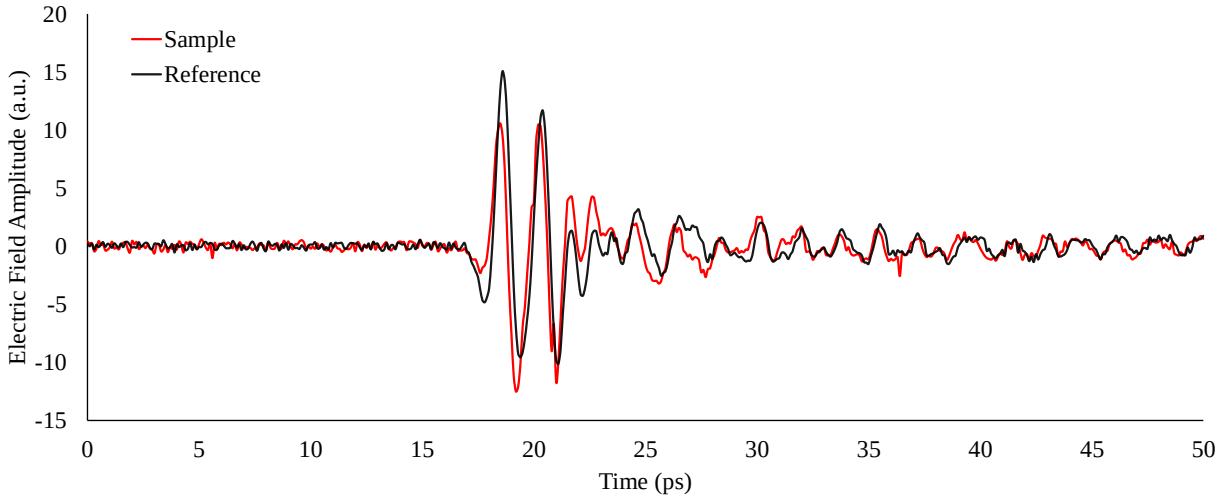

Figure 13. Reference and sample THz signals for obstructed electron density measurement.

VI. Conclusion

THz-TDS is a novel plasma diagnostic capable of providing line-integrated electron number density in Hall thruster and other EP plasmas. This work has demonstrated the theoretical applicability of THz-TDS to EP plasmas and provided a demonstration of the HPEPL THz-TDS system. Specifically, this work has shown that THz-TDS is a viable tool for measuring electron density *through* boron nitride. The many advantages provided by THz-TDS, including its insensitivity to mechanical vibrations, sub-nanosecond THz pulse duration, and transmissibility of THz radiation through boron nitride will enable the technique to investigate plasma phenomena not presently accessible to other optical diagnostics.

Acknowledgments

Nathan Brown is supported by the National Science Foundation Graduate Research Fellowship under grant number DGE-1650044, an Achievement Reward for College Scientists award, and the Georgia Tech Institute for Materials Graduate Student Fellowship. The authors would also like to thank Brandon Sforzo, Cameron Miller, Wyatt Amacker, Collin Whittaker, and Muhannad Eladl for their helpful discussions and assistance with setting up the experiments.

Appendix

A. Derivation of Standard THz-TDS Relations

The electric field of the broadband THz pulse is modeled as a superposition of one-dimensional plane waves of various frequencies transmitting through linear dielectric media with no reflections. The magnetic field is discarded because, unless charged particles in the medium move at relativistic speeds, its impact is negligible. Represented in the time (t) domain at a position (z) as $E(z,t)$, the electric field is cast to the frequency (ω) domain to $\hat{E}(z,\omega)$ through the Fourier transform by Eq. (9).

$$\hat{E}(z,\omega) = \int_{-\infty}^{\infty} E(z,t)\exp[-i\omega t]\,\mathrm{d}t \tag{9}$$

If the pulse enters a medium at $z = 0$ and propagates a distance L, the resulting and original electric fields in the spectral domain are related by Eq. (10).

$$\hat{E}(L,\omega) = \hat{E}(0,\omega)G(\omega)\exp\left[i\check{k}(\omega)\,L\right] \tag{10}$$

G is the frequency response of the entire THz-TDS system. It is included in Eq. (10) because the THz spectrometer is not a perfect measurement device and its response must be included as a convolution with the actual THz field. $\check{k}$ is the complex k-vector magnitude and is related to the real vacuum k-vector magnitude (k) and sample refractive index (n) and absorption coefficient (α) by Eq. (11).

$$\check{k}(\omega) = k(\omega)\ + k(\omega)\,[n(\omega) - 1] + i\frac{\alpha(\omega)}{2} \tag{11}$$

The real vacuum k-vector magnitude is defined by Eq. (12), where c is the speed of light.

$$k(\omega)\ = \frac{\omega}{c} \tag{12}$$

When THz-TDS is performed, a reference pulse, $\hat{E}_{ref}(\omega)$, is measured after propagation through vacuum and a sample pulse, $\hat{E}_{sam}(\omega)$, is measured after propagation through the sample of interest. Using Eq. (10), the measured reference and sample pulses can therefore be expressed by Eq. (13).

$$\begin{aligned}\hat{E}_{ref}(\omega) &= \hat{E}_{gen}(\omega)G(\omega)\exp[ik(\omega)\,L]\\ \hat{E}_{sam}(\omega) &= \hat{E}_{gen}(\omega)G(\omega)\exp\left[i\check{k}(\omega)L\right]\end{aligned} \tag{13}$$

Taking the ratio of the two resulting complex spectra yields Eq. (14) and effectively eliminates measurement dependence on the generated THz radiation and THz spectrometer response.

$$\frac{\hat{E}_{sam}(\omega)}{\hat{E}_{ref}(\omega)} = \exp\left[iL\left[\check{k}(\omega) - k(\omega)\ \right]\right] \tag{14}$$

Substituting in the expression for $\check{k}$ from Eq. (11) and re-arranging yields Eqs. (2) and (3) above.[14]

B. Derivation of THz-TDS Relations for Propagation through Plasma

Consider an infinite, uniform, and unmagnetized Lorentz plasma in which electrons are assumed to move through a stationary "fluid" of ions and neutrals and may only interact with each other through collective space charge. Further

assume that the interaction between electrons and the background fluid may be approximated as viscous damping, properties dependent upon electron temperature can be neglected, and the motion of a single electron is representative of the behavior of all electrons in the plasma. Under these assumptions, the spatial displacement of an electron (ξ), under forcing from a spatially invariant electric field (E) can be modeled as a damped harmonic oscillator by Eq. (15).

$$m_e \frac{\partial^2 \xi(t)}{\partial t^2} + \nu m_e \frac{\partial \xi(t)}{\partial t} = -eE(t) \tag{15}$$

m_e and e are the mass and charge, respectively, of the electron and ν is the damping coefficient, which can be interpreted physically as the average plasma momentum transfer collision rate. Assuming all quantities oscillate in time as $\exp(-i\omega t)$, the Fourier transform allows for the steady-state solution to be determined in the spectral domain by letting $\partial/\partial t \rightarrow -i\omega$ as in Eq. (16).

$$m_e(-i\omega)^2 \xi(\omega) + \nu m_e(-i\omega)\xi(\omega) = -eE(\omega) \tag{16}$$

Re-arranging produces Eq. (17).

$$\xi(\omega) = \frac{eE(\omega)}{m_e \omega(\omega + i\nu)} \tag{17}$$

The resulting complex current density, ($\breve{J}$), can be determined through multiplication of the charge density ($-n_e e$) and the electron velocity in the spectral domain ($-i\omega\xi$) and is given by Eq. (18), where n_e is the electron number density.

$$\breve{J}(\omega) = -n_e e(-i\omega)\xi(\omega) = \frac{i n_e e^2}{m_e(\omega + i\nu)} E(\omega) \tag{18}$$

The complex dielectric constant ($\breve{\varepsilon}$) is therefore given by Eq. (19), where $\breve{\sigma}$ is the complex conductivity and ϵ_0 is the permittivity of free space.

$$\breve{\varepsilon}(\omega) = 1 + i\frac{\breve{\sigma}(\omega)}{\omega\epsilon_0} = 1 + i\frac{\breve{J}(\omega)}{\omega\epsilon_0 E(\omega)} = 1 - \frac{n_e e^2}{\omega\epsilon_0 m_e(\omega + i\nu)} \tag{19}$$

Written in terms of the plasma frequency (ω_p), Eq. (19) becomes Eq. (20).

$$\breve{\varepsilon}(\omega) = 1 - \frac{\omega_p^2}{\omega(\omega + i\nu)} \tag{20}$$

Splitting the real and imaginary parts of the complex dielectric constant yields Eq. (21).

$$\breve{\varepsilon}(\omega) = 1 - \frac{\omega_p^2}{\omega^2 + \nu^2} + i\left(\frac{\omega_p^2 \nu}{\omega[\omega^2 + \nu^2]}\right) \tag{21}$$

The complex dielectric constant is related to the complex index of refraction by Eq. (22).

$$\breve{\varepsilon}(\omega) = \breve{n}^2(\omega) \tag{22}$$

Letting ε_R and ε_I be the real and imaginary parts of $\breve{\varepsilon}$, respectively, and n_R and n_I be the real and imaginary parts of $\breve{n}$, respectively, Eq. (23) holds.

$$(n_R + in_I)^2 = \varepsilon_R + i\varepsilon_I \tag{23}$$

Equating the real and imaginary parts in Eq. (23) yields the system in Eq. (24).

$$\begin{aligned} n_R^2 - n_I^2 &= \varepsilon_R \\ 2n_R n_I &= \varepsilon_I \end{aligned} \tag{24}$$

The real and imaginary parts of the complex refractive index can therefore be expressed in terms of the real and imaginary parts of the complex dielectric constant by Eq. (25).

$$\begin{aligned} n_R &= \sqrt{\frac{\varepsilon_R + \sqrt{\varepsilon_R^2 + \varepsilon_I^2}}{2}} \\ n_I &= \sqrt{\frac{-\varepsilon_R + \sqrt{\varepsilon_R^2 + \varepsilon_I^2}}{2}} \end{aligned} \tag{25}$$

Substituting Eq. (21) into Eq. (25) yields Eq.(26), which gives the complex refractive index in terms of the plasma parameters and applied electric field.

$$\begin{aligned} \breve{n}(\omega) = &\sqrt{\frac{1}{2}\left(1 - \frac{\omega_p^2}{\omega^2 + \nu^2}\right) + \frac{1}{2}\sqrt{\left(1 - \frac{\omega_p^2}{\omega^2 + \nu^2}\right)^2 + \left(\frac{\omega_p^2 \nu}{\omega[\omega^2 + \nu^2]}\right)^2}} \\ &+ i\sqrt{-\frac{1}{2}\left(1 - \frac{\omega_p^2}{\omega^2 + \nu^2}\right) + \frac{1}{2}\sqrt{\left(1 - \frac{\omega_p^2}{\omega^2 + \nu^2}\right)^2 + \left(\frac{\omega_p^2 \nu}{\omega[\omega^2 + \nu^2]}\right)^2}} \end{aligned} \tag{26}$$

The complex refractive index is related to the complex k-vector magnitude by Eq. (27).

$$\check{k}(\omega) = \frac{\omega}{c}\,\check{n}(\omega) \tag{27}$$

Substituting Eq. (26) into Eq. (27) yields Eq. (28).

$$\begin{aligned}\check{k}(\omega) = \frac{\omega}{c}\sqrt{\frac{1}{2}\left(1-\frac{\omega_p^2}{\omega^2+\nu^2}\right)+\frac{1}{2}\sqrt{\left(1-\frac{\omega_p^2}{\omega^2+\nu^2}\right)^2+\left(\frac{\omega_p^2\nu}{\omega[\omega^2+\nu^2]}\right)^2}} \\ +\frac{i\omega}{c}\sqrt{-\frac{1}{2}\left(1-\frac{\omega_p^2}{\omega^2+\nu^2}\right)+\frac{1}{2}\sqrt{\left(1-\frac{\omega_p^2}{\omega^2+\nu^2}\right)^2+\left(\frac{\omega_p^2\nu}{\omega[\omega^2+\nu^2]}\right)^2}}\end{aligned} \tag{28}$$

Substituting Eq. (28) into Eq. (14) and re-arranging to the form of Eq. (2) yields Eq. (29).

$$A(\omega) = \exp\left[-\frac{\omega L}{c}\sqrt{-\frac{1}{2}\left(1-\frac{\omega_p^2(z)}{\omega^2+\nu^2(z)}\right)+\frac{1}{2}\sqrt{\left(1-\frac{\omega_p^2(z)}{\omega^2+\nu^2(z)}\right)^2+\left(\frac{\omega_p^2(z)\nu(z)}{\omega[\omega^2+\nu^2(z)]}\right)^2}}\right]$$

$$\Phi(\omega) = \frac{\omega L}{c}\left[\sqrt{\frac{1}{2}\left(1-\frac{\omega_p^2(z)}{\omega^2+\nu^2(z)}\right)+\frac{1}{2}\sqrt{\left(1-\frac{\omega_p^2(z)}{\omega^2+\nu^2(z)}\right)^2+\left(\frac{\omega_p^2(z)\nu(z)}{\omega[\omega^2+\nu^2(z)]}\right)^2}}-1\right] \tag{29}$$

Relaxing the assumption of a uniform plasma and instead assuming the plasma properties do not vary significantly on the scale of the radiation wavelength enables use of the Wentzel–Kramers–Brillouin (WKB) approximation. Expressions for the amplitude and phase are converted to integrals along the THz path and become Equation (4) given above.[17]

References

[1]Jamison, S. P., Shen, J., Jones, D. R., Issac, R. C., Ersfeld, B., Clark, D., and Jaroszynski, D. A., "Plasma characterization with terahertz time–domain measurements," *Journal of Applied Physics*, Vol. 93, No. 7, 2003, pp. 4334-4336.
doi: 10.1063/1.1560564

[2]Kolner, B. H., Conklin, P. M., Buckles, R. A., Fontaine, N. K., and Scott, R. P., "Time-resolved pulsed-plasma characterization using broadband terahertz pulses correlated with fluorescence imaging," *Applied Physics Letters*, Vol. 87, No. 15, 2005, Paper 151501.
doi: 10.1063/1.2103421

[3]Mics, Z., Kadlec, F., Kužel, P., Jungwirth, P., Bradforth, S. E., and Apkarian, V. A., "Nonresonant ionization of oxygen molecules by femtosecond pulses: Plasma dynamics studied by time-resolved terahertz spectroscopy," *The Journal of Chemical Physics*, Vol. 123, No. 10, 2005, Paper 104310.
doi: 10.1063/1.2032987

[4]Ebbinghaus, S., Schröck, K., Schauer, J. C., Bründermann, E., Heyden, M., Schwaab, G., Böke, M., Winter, J., Tani, M., and Havenith, M., "Terahertz time-domain spectroscopy as a new tool for the characterization of dust forming plasmas," *Plasma Sources Science and Technology*, Vol. 15, No. 1, 2006, pp. 72-77.
doi: 10.1088/0963-0252/15/1/011

[5]Ando, A., Kurose, T., Reymond, V., Kitano, K., Kitahara, H., Takano, K., Tani, M., Hangyo, M., and Hamaguchi, S., "Electron density measurement of inductively coupled plasmas by terahertz time-domain spectroscopy (THz-TDS)," *Journal of Applied Physics*, Vol. 110, No. 7, 2011, Paper 073303.
doi: 10.1063/1.3633488

[6]Jang, D., Uhm, H. S., Jang, D., Hur, M. S., and Suk, H., "Electron density characterization of inductively-coupled argon plasmas by the terahertz time-domain spectroscopy," *Plasma Sources Science and Technology*, Vol. 25, No. 6, 2016, Paper 065008. doi: 10.1088/0963-0252/25/6/065008

[7]Kang, K., Jang, D., and Suk, H., "Plasma density measurements using THz pulses from laser-plasmas," *Journal of Instrumentation*, Vol. 12, No. 11, 2017, Paper C11003.
doi: 10.1088/1748-0221/12/11/C11003

[8]Meier, S. M., Tsankov, T. V., Luggenhölscher, D., and Czarnetzki, U., "Measurement of plasma densities by dual frequency multichannel boxcar THz time domain spectroscopy," *Journal of Physics D: Applied Physics*, Vol. 50, No. 24, 2017, Paper 245202. doi: 10.1088/1361-6463/aa708f

[9]Meier, S. M., Hecimovic, A., Tsankov, T. V., Luggenhölscher, D., and Czarnetzki, U., "First measurements of the temporal evolution of the plasma density in HiPIMS discharges using THz time domain spectroscopy," *Plasma Sources Science and Technology*, Vol. 27, No. 3, 2018, Paper 035006.
doi: 10.1088/1361-6595/aab188

[10]Gatesman, A. J., Giles, R. H., and Waldman, J., "Submillimeter optical properties of hexagonal boron nitride," *Journal of Applied Physics*, Vol. 73, No. 8, 1993, pp. 3962-3966.
doi: 10.1063/1.352860

[11]Naftaly, M., and Leist, J., "Investigation of optical and structural properties of ceramic boron nitride by terahertz time-domain spectroscopy," *Applied Optics*, Vol. 52, No. 4, 2013, pp. B20-B25.
doi: 10.1364/AO.52.000B20

[12]Hecht, E., *Optics, 5th ed.*, Pearson, Malaysia, 2017, pp. 18-150.

[13]Hangyo, M., Nagashima, T., and Nashima, S., "Spectroscopy by pulsed terahertz radiation," *Measurement Science and Technology*, Vol. 13, No. 11, 2002, pp. 1727-1738.
doi: 10.1088/0957-0233/13/11/309

[14]Dexheimer, S. L., ed., *Terahertz Spectroscopy: Principles and Applications*, CRC Press, Boca Raton, FL, 2008, pp. 1-72.

[15]Lee, Y.-S., *Principles of Terahertz Science and Technology*, Springer, New York, 2009, pp. 1-116.

[16]Neu, J., and Schmuttenmaer, C. A., "Tutorial: An introduction to terahertz time domain spectroscopy (THz-TDS)," *Journal of Applied Physics*, Vol. 124, No. 23, 2018, Paper 231101.
doi: 10.1063/1.5047659

[17]Heald, M. A., and Wharton, C. B., *Plasma Diagnostics with Microwaves*, John Wiley & Sons Inc., New York, 1965, pp. 1-452.

[18]Hutchinson, I. H., *Principles of Plasma Diagnostics*, Cambridge University Press, New York, 2002, pp.104-143.

[19]Janson, S., "Microwave Interferometry for Ion Engines," *30th Joint Propulsion Conference and Exhibit*, American Institute of Aeronautics and Astronautics, AIAA Paper 94-2741, 1994.
doi: 10.2514/6.1994-2741

[20]Ohler, S. G., Gilchrist, B. E., and Gallimore, A. D., "Nonintrusive Electron Number Density Measurements in the Plume of a 1 kW Arcjet Using a Modern Microwave Interferometer," *IEEE Transactions on Plasma Science*, Vol. 23, No. 3, 1995, pp. 428-435.
doi: 10.1109/27.402337

[21]Gilchrist, B. E., Ohler, S. G., and Gallimore, A. D., "Flexible microwave system to measure the electron number density and quantify the communications impact of electric thruster plasma plumes," *Review of Scientific Instruments*, Vol. 68, No. 2, 1997, pp. 1189-1194.
doi: 10.1063/1.1147882

[22]Ohler, S., Gilchrist, B. E., and Gallimore, A., "Microwave Plume Measurements of a Closed Drift Hall Thruster," *Journal of Propulsion and Power*, Vol. 14, No. 6, 1998, pp. 1016-1021.
doi: 10.2514/2.5367

[23]Cappelli, M. A., Gascon, N., and Hargus, W. A., "Millimetre wave plasma interferometry in the near field of a Hall plasma accelerator," *Journal of Physics D: Applied Physics*, Vol. 39, No. 21, 2006, pp. 4582-4588.
doi: 10.1088/0022-3727/39/21/013

[24]Diels, J.-C., and Rudolph, W., *Ultrashort Laser Pulse Phenomena, 2nd Ed.*, Elsevier, Boston, MA, 2006, pp. 1-136.

[25]Auston, D. H., Cheung, K. P., and Smith, P. R., "Picosecond photoconducting Hertzian dipoles," *Applied Physics Letters*, Vol. 45, No. 3, 1984, pp. 284-286.
doi: 10.1063/1.95174

[26]Jepsen, P. U., Jacobsen, R. H., and Keiding, S. R., "Generation and detection of terahertz pulses from biased semiconductor antennas," *Journal of the Optical Society of America B*, Vol. 13, No. 11, 1996, pp. 2424-2436.
doi: 10.1364/JOSAB.13.002424

[27]Van Rudd, J., and Mittleman, D. M., "Influence of substrate-lens design in terahertz time-domain spectroscopy," *Journal of the Optical Society of America B*, Vol. 19, No. 2, 2002, pp. 319-329.
doi: 10.1364/JOSAB.19.000319

[28]Planken, P. C. M., Nienhuys, H.-K., Bakker, H. J., and Wenckebach, T., "Measurement and calculation of the orientation dependence of terahertz pulse detection in ZnTe," *Journal of the Optical Society of America B*, Vol. 18, No. 3, 2001, pp. 313-317.
doi: 10.1364/JOSAB.18.000313

[29]Wu, Q., and Zhang, X. C., "Free-space electro-optic sampling of terahertz beams," *Applied Physics Letters*, Vol. 67, No. 24, 1995, pp. 3523-3525.
doi: 10.1063/1.114909
[30]Wu, Q., Litz, M., and Zhang, X. C., "Broadband detection capability of ZnTe electro-optic field detectors," *Applied Physics Letters*, Vol. 68, No. 21, 1996, pp. 2924-2926.
doi: 10.1063/1.116356
[31]Gallot, G., and Grischkowsky, D., "Electro-optic detection of terahertz radiation," *Journal of the Optical Society of America B*, Vol. 16, No. 8, 1999, pp. 1204-1212.
doi: 10.1364/JOSAB.16.001204
[32]van Exter, M., Fattinger, C., and Grischkowsky, D., "Terahertz time-domain spectroscopy of water vapor," *Optics Letters*, Vol. 14, No. 20, 1989, pp. 1128-1130.
doi: 10.1364/OL.14.001128
[33]Goebel, D. M., and Katz, I., *Fundamentals of Electric Propulsion: Ion and Hall Thrusters*, John Wiley & Sons, Hoboken, New Jersey, 2008, pp. 1-442.